Contemporary stress orientations in the Andean retroarc between 34°S and 39°S from borehole breakout analysis

C. Guzmán,[1] E. Cristallini,[1,2] and G. Bottesi[3]

Received 27 February 2006; revised 15 February 2007; accepted 16 March 2007; published 27 June 2007.

[1] In this paper we present the results of the analysis of borehole breakouts from 115 wells drilled within Neuquén Basin in the Andean retroarc between 34° and 39°S (Argentina). The first-order present-day stress orientation in the Andean retroarc is expected to be mainly controlled by the plate boundary forces (azimuth 80°) and the topographic forces (E–W). The obtained maximum horizontal stress (SH_{max}) has a preferred trend with a resultant direction of azimuth 88.7° and a 95% confidence interval of 13.3° consistent with the expected trend. The horizontal stress trajectory map achieved for this region shows that the SH_{max} along the study area is not completely uniform. To the north of Colorado River, the SH_{max} shows an ESE tendency interpreted as significant influenced by the topographic forces. To the south of Colorado River, SH_{max} has an ENE trend similar to the expected based on plate boundary forces. To the southeast of the region, a NE direction was found, probably showing a basement structural control in the stress field geometry. The stress orientations obtained for the whole region show that plate boundary forces, drag basal, and topographic forces are strongly controlling the stress direction distribution.
Citation: Guzmán, C., E. Cristallini, and G. Bottesi (2007), Contemporary stress orientations in the Andean retroarc between 34°S and 39°S from borehole breakout analysis, *Tectonics*, *26*, TC3016, doi:10.1029/2006TC001958.

1. Introduction

[2] A comprehensive knowledge of regional stress directions is not only important in scientific terms and earthquake hazard assessment but also gives important information for optimizing petroleum recovery and exploration of fracture related reservoirs [*Fuchs and Müller*, 2001]. The identification of global, regional and local patterns of stress distribution provides new insight into mountain building, evolution of sedimentary basins and characterization of active faults with earthquake potential [*Zoback*, 1992; *Tingay et al.*, 2005].

[3] *Zoback et al.* [1989] started with the World Stress Map Project compiling information from different sources of stress directions measured in continental crust around the world [*Zoback*, 1992; J. Reinecker et al., The 2005 release of the World Stress Map, 2005, available at http://www.world-stress-map.org]. The map in Figure 1 shows the direction of the maximum horizontal stress (SH_{max}) for South America compiled by the World Stress Map (J. Reinecker et al., The 2005 release of the World Stress Map, 2005, available at http://www.world-stress-map.org). Most of the information comes from earthquake focal mechanisms and geological field observations of recent and active faulting, and fewer data from borehole breakouts and volcanic alignments. Different authors have provided geologic information contributing with the knowledge of stress distribution, intensity and direction within this Andean region [e.g., *Cobbold et al.*, 1999; *Lavenu and Cembrano*, 1999a, 1999b; *Cortés*, 2000; *Folguera et al.*, 2002]; however, no good data have been published about current stress direction distribution.

[4] To the southwest of the region analyzed in this study, *Lavenu and Cembrano* [1999a] examined the spatial distribution of the stress states during the Pliocene and Pleistocene in the Chilean Andes between the 38° and 42°30′S. They determined two tectonic events: (1) Pliocene compressive event characterized by a maximum compressional stress roughly oriented with an E–W direction and (2) Pleistocene event with stress partitioning where the fore arc has a NNE to S–N principal stress orientation and the intra-arc zone has a NE principal stress direction.

[5] *Coblentz and Richardson* [1996] and *Meijer et al.* [1997] modeled the stress field acting in the South American plate. *Coblentz and Richardson* [1996] made three different stress models; they concluded that the stress field in the South American plate results from the interaction of two principal tectonic processes, the buoyancy or topographic forces and compressional stresses transmitted across plate boundaries. They proposed that the origin of the E–W compressive stress regime is the result of the interaction between the ridge push force and the collisional forces acting along the western margin. The approach of *Meijer et al.* [1997] is an improvement of previous work on the Andes [e.g., *Dalmayarc and Molnar*, 1981; *Richardson and Coblentz*, 1994] in which the state of the stress in the mountain range has been addressed only in terms of vertical cross section. Their models also have some differences with *Coblentz and Richardson*'s [1996] model, especially because different types of forces are included. *Meijer et*

[1]Laboratorio de Modelado Geológico, Departamento de Ciencias Geológicas, Universidad de Buenos Aires, Buenos Aires, Argentina.
[2]Consejo Nacional de Investigaciones Científicas y Técnicas, Buenos Aires, Argentina.
[3]Repsol YPF, Buenos Aires, Argentina.

0278-7407/07/2006TC001958$12.00

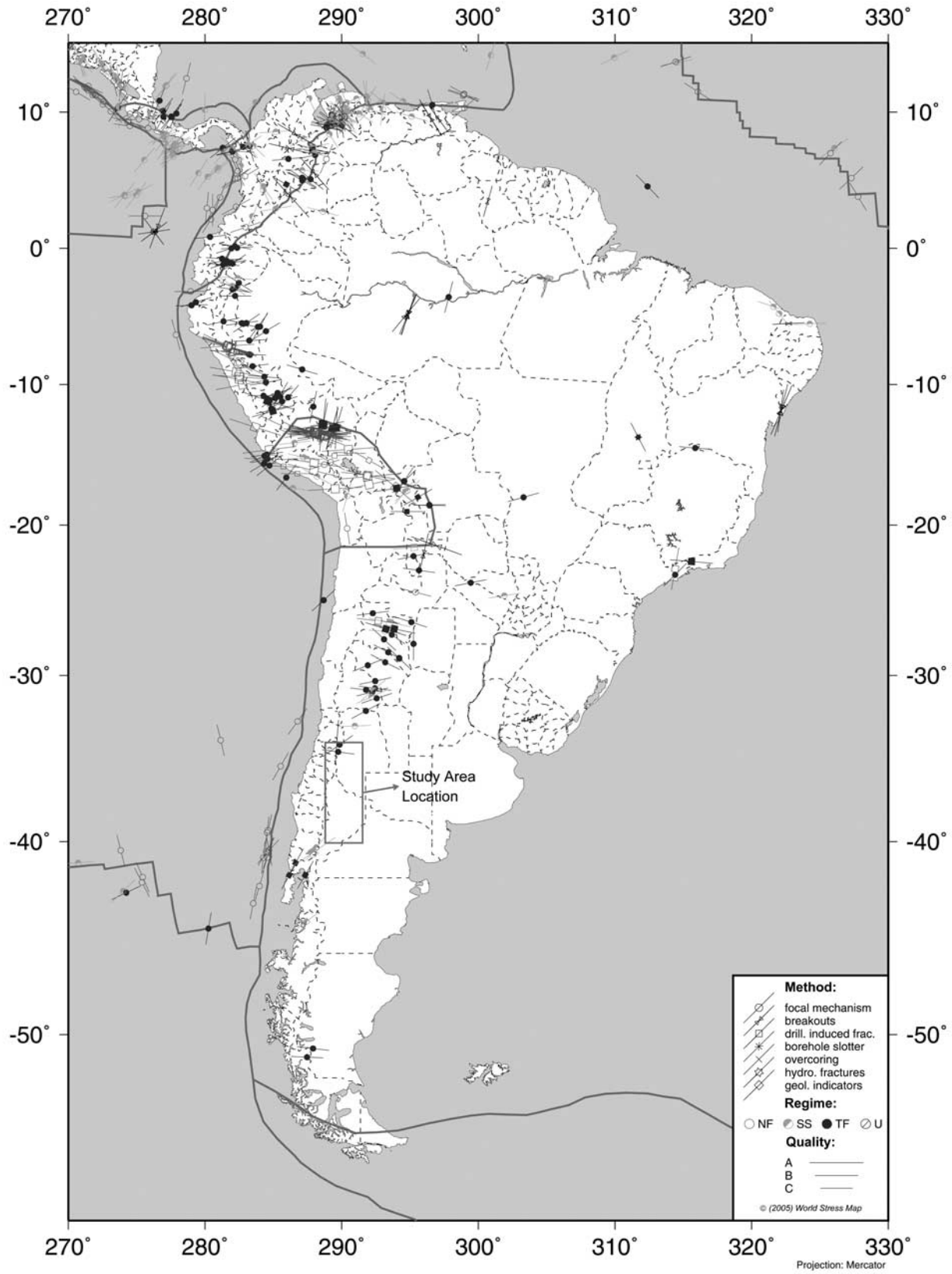
270°
280°
290°
300°
310°
320°
330°
10°
0°
-10°
-20°
-30°
-40°
-50°
Study Area
Location
Method:
focal mechanism
breakouts
drill. induced frac.
borehole slotter
overcoring
hydro. fractures
geol. indicators
Regime:
NF SS TF U
Quality:
A
B
C
© (2005) World Stress Map
Projection: Mercator

Figure 1

al. [1997] concluded that a uniform distribution of the resistance on the western margin of South America provides a better overall fit to the available observations than a dip-dependent distribution of resistance magnitude. Their results also suggest that an extra driving force, additional to ridge push, may be acting on the South American Plate to ''sustain'' the Andean Cordillera.

[6] Although several authors have been contributing with actual stress data within South America, still few data are available especially for the retroarc of southern South America. Therefore the purpose of this paper is to introduce further information of the horizontal stress acting in the Andean retroarc between 34° and 39°S, providing a large amount of borehole breakout data for South America. An analysis of the obtained results is presented and discussed taking into account the existing plate-wide scale numerical models which predict the stress orientation. In order to obtain the horizontal stress field, borehole breakout orientations calculated using four-arm caliper data from 115 wells drilled within Neuquén Basin in Argentina, were used. Horizontal stress directions, calculated for the retroarc, were used to estimate the differences between the obtained stress field and the expected one, based on the present convergence vector, the direction of the ridge push and the topographic forces. A discussion of these differences is presented taking into account the geological and structural features of the region.

2. Tectonic Setting

[7] The wells used for this study were drilled within the Neuquén Basin, in the retroarc of the Central Andes between 34°S and 39°S. The Neuquén Basin constitutes one of the major producers of oil and gas in Argentina. It consists of 2000–6000 m thick Mesozoic synrift and postrift continental and marine deposits locally overlaid by moderately thick to thin Cretaceous and Tertiary foreland deposits [*Uliana et al.*, 1995].

[8] The Neuquén Basin, as many other basins, has a polygenetic origin [*Cobbold et al.*, 1999] and may be broadly considered a mainly marine retroarc basin from Early Jurassic to Early Cretaceous times [*Ramos*, 1989; *Vergani et al.*, 1995]. It became a foreland basin early in the Late Cretaceous as the result of the Andean uplift [*Zapata et al.*, 1999]. The development of the basin started in the Triassic as a rift-related basin with unconnected depocenters [*Mendiberri and Carbone*, 2002]. From the late Early Jurassic, to the Early Cretaceous, the sedimentation was characterized by sag facies related to thermal subsidence [*Turic et al.*, 1987] and controlled by global sea level changes [*Legarreta and Uliana*, 1996]. Nevertheless, some parts of the basin have been from time to time affected by local inversions and transpressions [*Uliana et al.*, 1995; *Vergani et al.*, 1995; *Pángaro et al.*, 2002; *Mosquera*, 2002; *Mosquera and Ramos*, 2005].

[9] In the early Late Cretaceous, evidence of compression and uplift were observed in the western part of the basin and continental deposits accumulated in a foreland tectonic setting [*Zamora Valcarce et al.*, 2005]. By this time, the sedimentation was influenced by arc and intra basin derived debris which may have reflected the regional arc uplift [*Legarreta et al.*, 1989] and an incipient development of a fold and thrust belt [*Barrio*, 1990]. The structure and uplift of this western fold and thrust belt began in the early Late Cretaceous at about 100 Ma [*Zapata et al.*, 1999; *Zamora Valcarce et al.*, 2005].

[10] The Andean fold and thrust belt between 34° and 39°S can be divided into three segments: The Malargüe fold and thrust belt in the north (from ~34° to ~36°30′S), the Agrio fold belt in the south (~37°30′ to ~39°S) and the Barrancas-Colorado segment between ~36°30′S and ~37°30′S (Figure 2).

[11] The northern and central sectors (Malargüe and Barrancas-Colorado) are characterized by NNE trending structures clearly involving large basement blocks. In contrast, the southern segment (Agrio fold belt) is characterized by smaller NNW trending structures where the basement is incipiently involved. Traditionally, the participation of the Permo-Triassic volcaniclastic basement (Choiyoi Group) in the deformation is explained as a Cretaceous-Tertiary tectonic inversion of Triassic extensional half graben faults [*Kozlowski et al.*, 1990, 1993; *Viñes*, 1990; *Kozlowski*, 1991; *Manceda and Figueroa*, 1995; *Ramos et al.*, 1996; *Ramos*, 1998; *Zapata et al.*, 1999]. However, some authors state that the basement is involved by low-angle thrust faults not related with the original normal faults [*Ploszkiewicz*, 1987; *Yagupsky et al.*, 2007].

[12] The recent tectonic history of this Andean region is particularly interesting. During the last 25 Ma, changes in the position of volcanic arc front and geochemistry suggest variations in the Wadati-Benioff geometry [*Muñoz and Stern*, 1988; *Stern*, 1989; *Ramos*, 1998; *Muñoz et al.*, 2000; *Folguera et al.*, 2002; *Kay*, 2005; *Ramos and Folguera*, 2005a]. A steep subduction zone was proposed between 25 and 15 Ma followed by a shallowing of the Wadati-Benioff zone in the Late Miocene. During the last 5 Ma, the Wadati-Benioff angle was steepened again and wide retroarc volcanism occurred within the study region [*Ramos and Folguera*, 2005b].

3. Borehole Breakout Analysis

[13] Borehole breakout formation has been extensively described in the literature [*Cox*, 1970; *Babcock*, 1978; *Bell*

Figure 1. World Stress Map for South America issue 2005. The orientations of the symbols are in the direction of the maximum horizontal stress (SH_{max}). The symbols represent different kinds of stress indicators and their length is a measure for the data quality. NF Normal faulting regime, SS strike slip faulting regime, TF thrust faulting regime (J. Reinecker et al., The 2005 release of the World Stress Map, 2005, available at http://www.world-stress-map.org). The area covered in this study has been outlined.

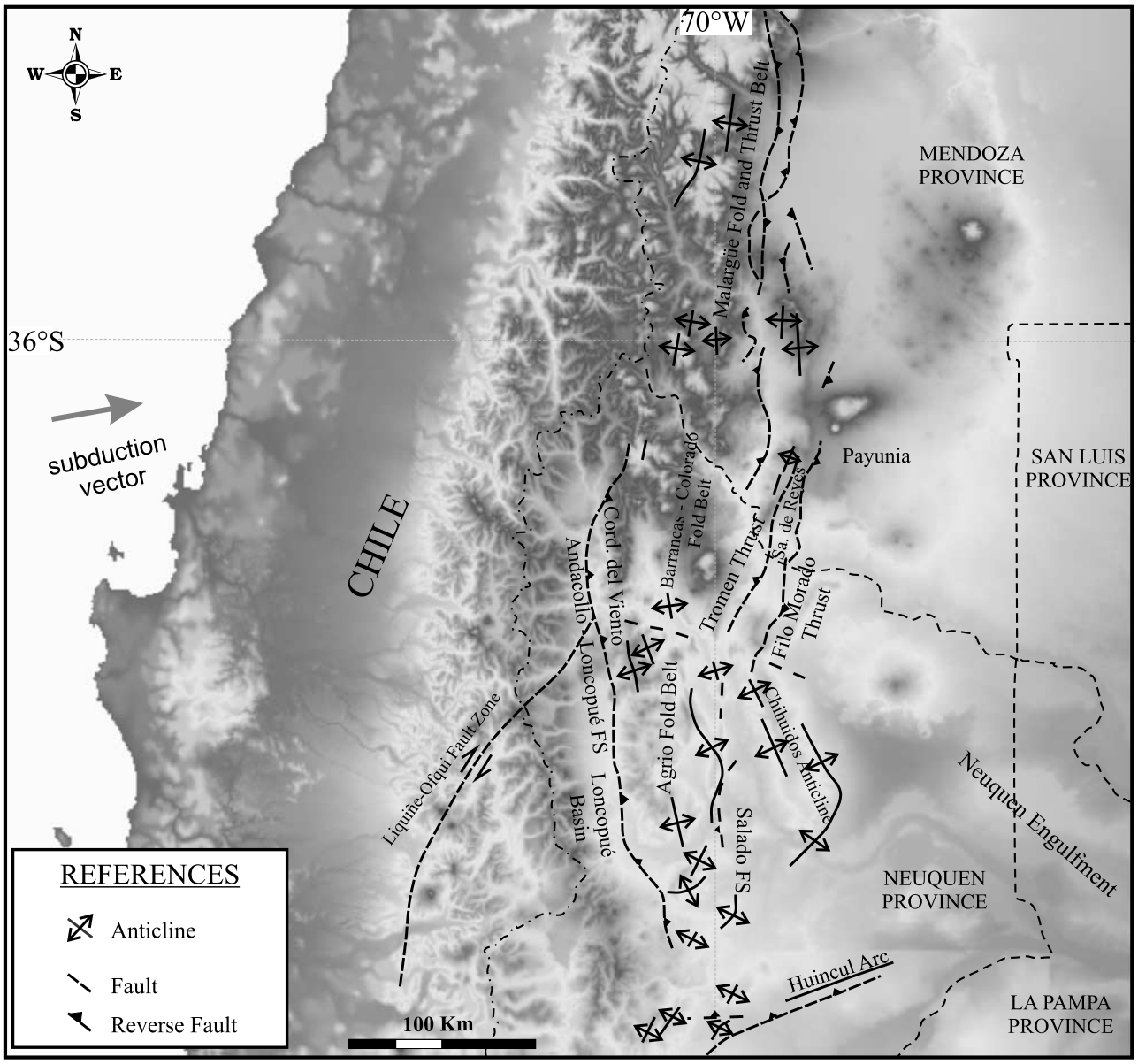

Figure 2. Major structures of the Neuquén Basin (modified after *Cobbold and Rossello* [2003]).

and Gough, 1979, 1982; *Gough and Bell*, 1979, 1981; *Zoback et al.*, 1985; *Plumb and Hickman*, 1985; *Bell and Babcock*, 1986; *Plumb and Cox*, 1987; *Zajac and Stock*, 1997]. Breakouts are stress-induced spalled regions on each side of the wellbore. It has been demonstrated that breakout orientation around a borehole is aligned with the least in situ horizontal stress [*Bell and Babcock*, 1986; *Plumb and Cox*, 1987] direction where the greatest compressive stress is concentrated [*Gough and Bell*, 1981; *Bell and Gough*, 1982; *Zerwer and Yassir*, 1994].

[14] The estimation of the principal horizontal stress directions using borehole breakouts is used by petroleum industry and drilling engineers to determine the stress regime for wellbore stability analyses and reservoir simulation. One of the oldest techniques for borehole breakout identification, first documented by *Cox* [1970], is using four-arm caliper data included in routine dipmeter logs. In the last years, more sophisticated and precise methods for breakout identification have been developed using borehole images (i.e., Ultrasonic Borehole Imager, Fullbore Formation Micro Imager Log, Full Bore Scanner Tool). However, the advantages of using four-arm caliper data to infer breakout orientations reside in the widespread occurrence of dipmeter information registered in deep exploration wells. The dipmeter logs are particularly useful in basins where the exploration period was concentrated when new techniques were not available. This is the case of Neuquén

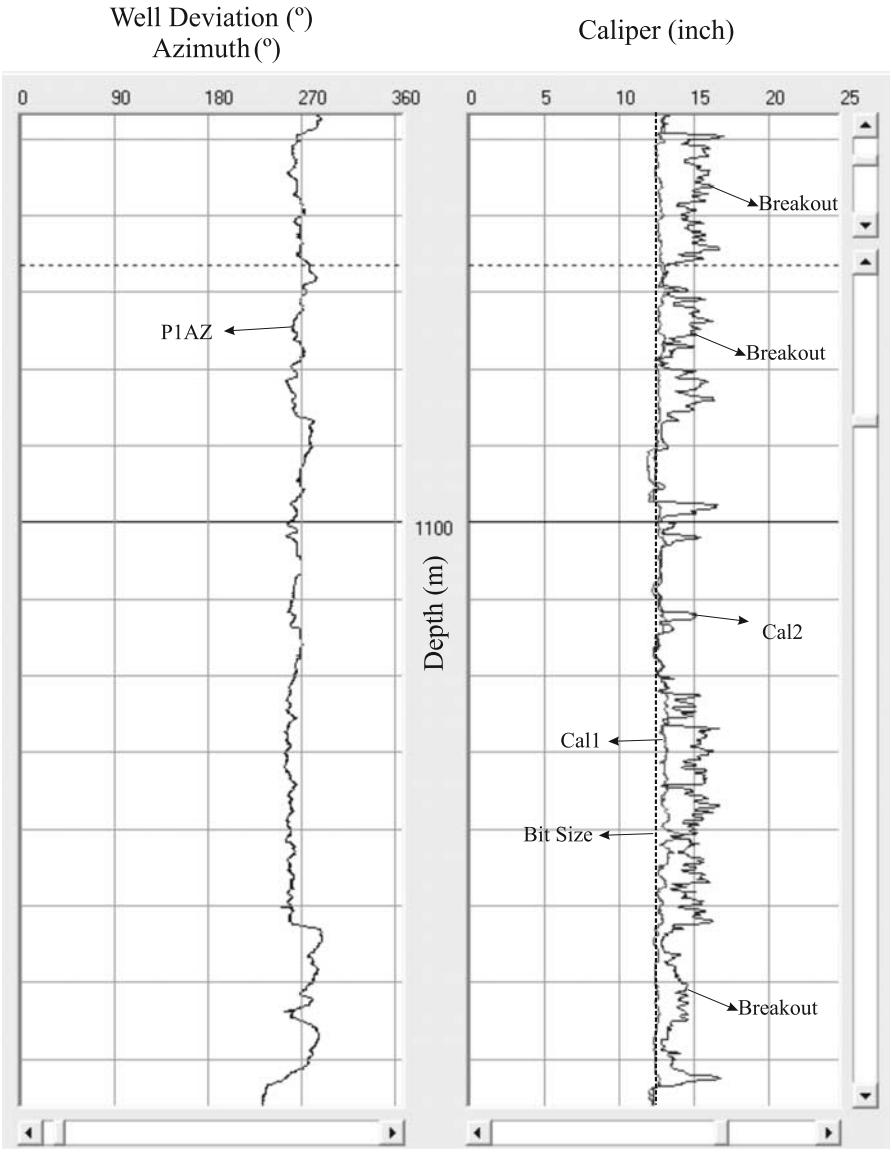

Figure 3. Example of four-arm caliper log plot showing borehole breakout interpreted following the six criteria used by the World Stress Map. Caliper two (Cal 2) locks into different breakout zones with an azimuth near 177° (P1AZ 267°). They suggest a SH_{max} direction of 87°.

Basin where the main exploration has been developed before 1990.

[15] To interpret borehole breakouts, four-arm dipmeter caliper logs were used. The dipmeter tool ascends rotating during log registration due to cable torque. Well diameter and reference arm orientation are continuously measured. When an elongation is present in the wellbore, the caliper pairs are differentially extended, the tool stops rotation and

Table 1. Quality Criterions Used by the World Stress Map Project[a]

Criterion	Description
A	Wells that have 10 or more distinct breakouts zones with a combined length >300 m and with a standard deviation ≤12°
B	Wells that have at least six distinct breakout zones with combined length >100 m and with standard deviation ≤20°
C	Wells that have at least four distinct breakout zones with a combined length >30 m and with standard deviation ≤25°
D	Wells that have less than four breakout zones or a combined length <30 m or with standard deviation >25°
E	Wells with no reliable breakouts detected or with extreme scatter of breakout orientations (standard deviation >40°)

[a]From *Sperner et al.* [2003].

Table 2. List of the 115 Wells Analyzed Within Mendoza and Neuquén Retroarc[a]

Well	Latitude	Longitude	Mean Breakout Direction Weighted by Length	Standard Deviation	Mean Breakout Direction Weighted by Number	Standard Deviation	Breakout Intervals	Meters Accumulated	Quality
1	−38.43	−68.06	28	3.0	27	3.0	2	120.0	D
2	−38.16	−68.65	4	4.3	4	4.2	19	411.8	A
3	-	-	0	1.5	1	1.6	2	7.3	D
4	−37.95	−69	9	0.0	9	0.0	1	7.3	D
5	−38.87	−69.06	169	2.9	172	3.8	2	7.0	D
6	−38.87	−69.07	167	16.6	179	17.7	5	159.0	C
7	−38.87	−69.05	168	5.8	172	7.4	2	67.1	D
8	−37.84	−68	47	30.8	50	52.7	3	57.5	D
9	−37.86	−67.84	36	14.4	33	17.8	7	130.3	B
10	−38.22	−68.53	155	21.9	168	14.3	11	225.6	C
11	−38.21	−68.52	161	7.0	160	8.5	3	52.5	D
12	−38.15	−68.31	10	18.2	8	18.6	7	20.7	B
13	−38.29	−68.07	130	10.6	140	19.8	3	123.0	D
14	−38.9	−69.55	157	27.9	155	41.9	5	105.3	D
15	−38.9	−69.57	163	45.3	172	39.2	10	286.5	E
16	−38.9	−69.48	17	30.4	4	24.7	9	85.9	D
17	−38.91	−69.5	39	7.2	38	8.2	11	59.3	C
18	−38.65	−68.26	139	10.2	142	9.8	32	299.8	A
19	−37.71	−68.63	152	0.0	152	0.0	1	23.8	D
20	−37.24	−69.35	148	11.1	150	26.3	18	387.8	A
21	−37.34	−69.41	175	7.9	172	12.5	3	34.3	D
22	−37.35	−69.31	168	9.7	166	13.1	33	2319.1	A
23	−38.63	−69.77	171	10.0	170	10.1	2	163.9	D
24	−37.61	−68.82	173	7.6	172	7.6	11	174.5	B
25	−37.78	−67.85	175	24.4	0	22.3	7	114.0	C
26	−37.34	−69.17	169	5.4	169	8.3	16	494.3	A
27	−37.7	−68.47	144	30.4	147	34.0	10	118.3	D
28	−37.66	−68.78	171	1.7	171	1.7	2	10.3	D
29	−37.18	−69.67	83	18.7	98	25.6	3	434.7	D
30	−37.15	−69.66	96	31.0	100	36.5	26	948.8	D
31	−37.32	−69.41	162	21.6	159	23.0	17	370.8	C
32	−37.27	−69.66	9	16.0	13	47.5	6	298.8	B
33	−37.27	−69.66	64	29.5	48	50.6	27	453.9	D
34	−37.28	−69.64	53	33.7	60	38.2	7	105.0	D
35	−38.43	−69.01	9	4.4	9	7.0	8	446.5	B
36	−39.04	−67.63	128	0.0	128	0.0	2	8.1	D
37	−38.69	−68.51	170	10.2	171	9.0	8	85.3	C
38	−38.35	−68.6	16	3.7	14	4.1	39	320.0	A
39	−39.24	−69.69	146	25.0	149	24.4	38	280.2	C
40	−37.29	−69.59	61	38.9	52	47.6	9	290.8	D
41	-	-	169	4.3	168	4.4	3	18.0	D
42	−37.19	−69.36	154	22.4	148	21.2	30	872.6	C
43	−37.17	−69.26	162	23.7	162	20.1	12	336.3	C
44	−38.08	−68.6	172	5.2	174	5.4	8	320.5	B
45	−38.54	−69.45	173	3.2	174	2.5	10	730.7	A
46	−39.14	−68.65	42	19.8	41	20.9	15	131.4	B
47	−39.11	−69.34	163	13.7	153	17.0	2	26.0	D
48	−37.14	−69.42	71	17.9	60	21.2	11	219.3	B
49	−37.12	−69.42	60	20.7	49	33.7	6	241.8	C
50	−37.13	−69.43	160	36.1	154	34.2	4	107.0	D
51	−35.74	−69.67	46	22.0	36	26.9	11	719.6	C
52	−37.11	−69.45	99	41.0	103	50.0	18	463.3	E
53	−35.87	−69.68	179	14.2	4	16.0	30	399.0	B
54	−35.82	−69.8	98	22.0	91	27.7	9	325.4	C
55	−35.19	−69.11	178	19.3	170	30.8	10	292.3	B
56	−36.98	−69.38	14	0.0	14	0.0	1	2.6	D
57	−36.13	−69.51	21	20.7	21	18.9	35	385.3	C
58	−36.12	−69.52	27	17.1	27	17.6	8	373.3	B
59	−37.29	−68.83	167	40.5	159	36.9	3	8.4	D
60	−36.2	−69.38	44	39.4	170	42.5	22	1598.1	D
61	−37.21	−69	165	7.3	165	6.0	8	223.0	B
62	−35.96	−69.84	145	44.9	167	45.1	16	331.8	E
63	−35.32	−69.71	73	24.2	66	41.2	8	534.7	C
64	−35.36	−69.72	112	23.4	113	40.3	7	698.1	C
65	−35.32	−69.71	21	31.2	18	30.0	4	237.5	D

Table 2. (continued)

Well	Latitude	Longitude	Mean Breakout Direction Weighted by Length	Standard Deviation	Mean Breakout Direction Weighted by Number	Standard Deviation	Breakout Intervals	Meters Accumulated	Quality
66	−35.29	−69.73	47	23.5	63	35.4	5	453.8	C
67	−35.36	−69.73	37	23.0	32	43.3	8	489.5	C
68	−36.68	−69.39	5	13.6	7	17.3	26	897.7	B
69	−37.09	−68.62	81	35.9	114	34.5	3	34.5	D
70	−36.1	−69.77	146	32.6	153	21.7	18	377.1	D
71	−37.1	−69.55	101	27.9	130	43.2	15	961.3	D
72	−37.07	−69.55	164	15.1	167	14.6	11	337.8	B
73	−38.91	−69.41	12	12.5	17	15.4	6	284.3	B
74	−35.94	−69.67	170	26.2	170	24.4	31	770.4	D
75	−37.1	−69.14	21	4.0	18	5.2	3	163.5	D
76	−35.47	−69.78	34	42.9	36	44.2	73	1297.2	E
77	−34.94	−69.51	14	20.0	14	26.4	17	642.5	B
78	−34.91	−69.52	161	41.8	113	33.0	4	87.0	E
79	−34.93	−69.52	8	11.5	8	11.5	2	233.0	D
80	−34.92	−69.52	14	14.1	11	24.5	7	559.8	B
81	−35.46	−69.34	176	32.4	174	39.6	3	24.3	D
82	−35.14	−69.69	46	46.5	33	45.8	15	358.3	E
83	−36.89	−69.2	15	10.6	22	18.2	6	171.0	B
84	−37.13	−69.44	17	49.4	154	27.3	19	464.5	E
85	−36.39	−69.76	163	5.8	164	8.5	10	845.1	A
86	−37.16	−69.15	164	7.5	160	17.4	9	376.1	B
87	−35.27	−69.65	26	12.7	24	27.8	11	1011.0	B
88	−36.82	−69.83	12	14.8	15	13.7	3	61.5	D
89	−36.2	−69.52	9	20.6	15	23.0	20	798.3	C
90	−36.19	−69.5	6	30.4	4	40.8	15	512.8	D
91	−37.09	−69.48	81	7.1	79	5.3	7	276.0	B
92	−37.13	−69.52	152	8.1	10	49.2	2	59.8	D
93	−35.81	−69.48	30	44.0	24	37.3	7	219.5	E
94	−34.68	−69.65	0	25.8	177	40.1	10	684.0	D
95	−34.68	−69.67	173	39.3	179	35.7	13	1222.0	D
96	−37.16	−69.48	8	39.1	17	53.7	15	481.3	D
97	−38.48	−67.93	164	2.6	164	2.9	6	23.0	D
98	−37.21	−69.25	138	65.4	158	38.1	7	123.8	E
99	−37.59	−69.76	16	19.0	12	28.2	5	413.0	C
100	−37.25	−69.1	150	32.3	150	29.5	14	438.8	D
101	−39.03	−69.35	68	40.3	76	43.4	10	207.3	E
102	−39.02	−69.35	18	25.3	21	41.8	9	206.5	D
103	−39.03	−69.37	159	20.8	155	25.1	6	53.0	C
104	−39.03	−69.36	150	23.5	148	23.1	8	153.3	C
105	−39.03	−69.16	178	43.5	160	35.2	4	496.1	E
106	−39.01	−69.13	152	3.8	155	4.6	2	90.0	D
107	−37.48	−69.84	31	19.7	26	23.2	8	45.8	C
108	−38.97	−69.42	172	15.0	175	21.9	8	244.5	B
109	−37.7	−68.92	161	20.0	158	23.2	18	548.8	B
110	−37.69	−68.92	131	46.9	68	57.5	12	119.0	E
111	−37.71	−68.94	166	14.6	173	11.9	15	192.0	B
112	−37.7	−68.88	169	5.4	169	8.1	14	160.0	B
113	−37.69	−68.92	10	28.1	180	46.2	3	36.5	D
114	-	-	1	0.0	1	0.0	1	6.8	D
115	−38.86	−69.95	153	28.3	152	38.7	19	1079.0	D

[a]For each well is shown the mean breakout orientation weighted by length and by number of breakout intervals, the standard deviation for the whole well and the quality using World Stress Map Project criterions (see Table 1).

a constant direction is recorded for the reference arm [*Zerwer and Yassir*, 1994]. Several authors enumerated different criteria to determine the borehole breakouts using dipmeter caliper data [e.g., *Plumb and Hickman*, 1985; *Zajac and Stock*, 1997]. In this study the breakout detection follows the criteria suggested by the World Stress Map (J. Reinecker et al., Borehole breakout analysis from four-arm caliper logs, 2004, http://www.world-stress-map.org): (1) Tool rotation must cease in the zone of enlargement. (2) There must be clear tool rotation into and out of the enlargement zone. (3) The smaller caliper reading is close to bit size; top and bottom of the breakout should be well marked. (4) Caliper difference has to exceed bit size by 10%. (5) The enlargement orientation should not coincide with the high side of the borehole in wells deviated by more

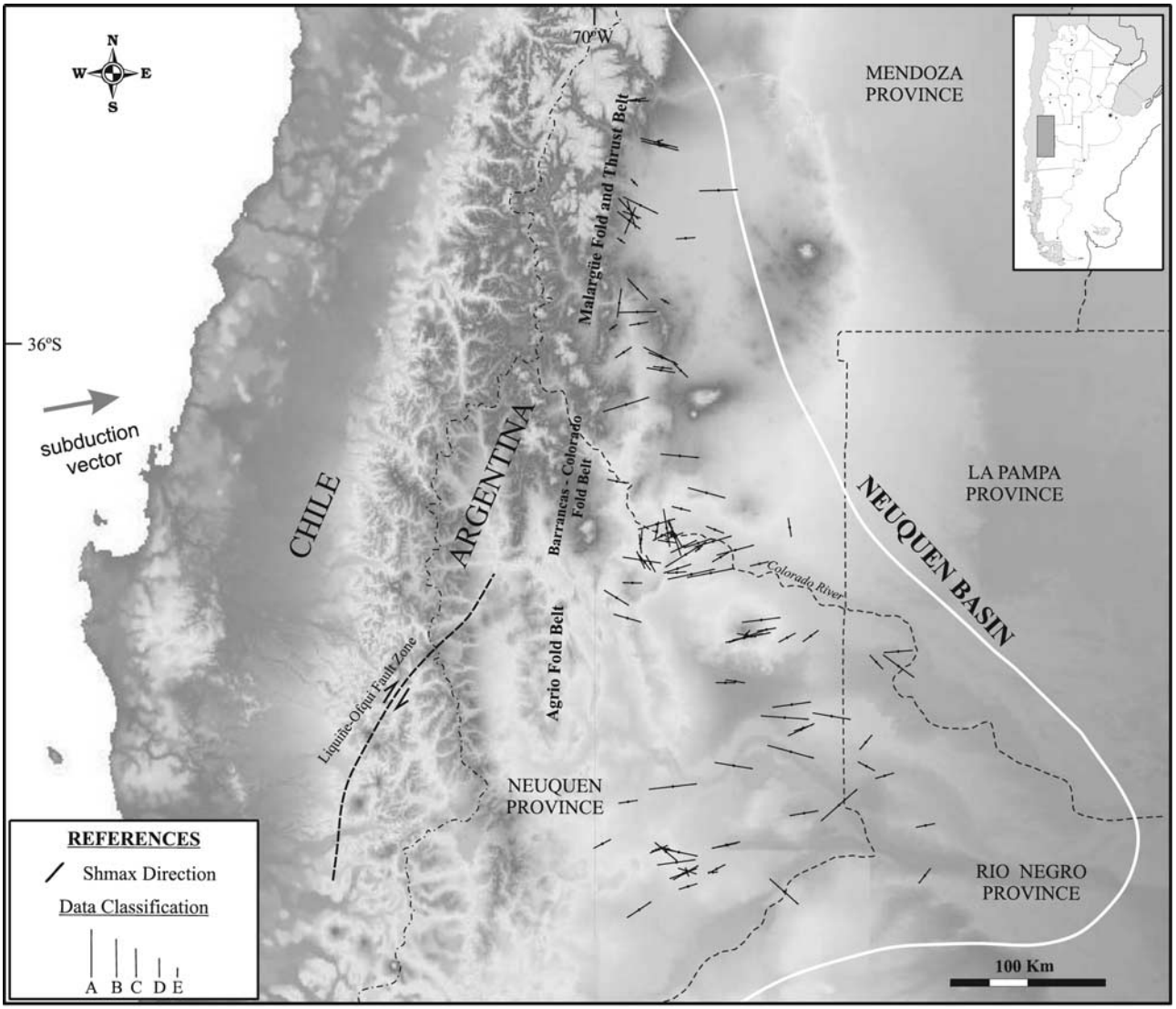

Figure 4. Orientation and classification of maximum horizontal stress from 115 bore wells within the Neuquén Basin. The different symbols correspond to SH_{max} classification using the World Stress Map criteria.

than 5°. (6) The length of enlargement zone must be greater than 1 m.

[16] The combined use of these six criteria enables to detect and distinguish zones of breakouts from other borehole enlargements such as washouts and key seats (J. Reinecker et al., Borehole breakout analysis from four-arm caliper logs, 2004, http://www.world-stress-map.org). In Figure 3, there is an example of four-arm caliper log plot showing borehole breakouts interpreted following the above criteria.

[17] The data have been ranked according to the World Stress Map quality ranking scheme [*Zoback and Zoback*, 1989, 1991; *Sperner et al.*, 2003]. The classification allows the comparison of different indicators (e.g., focal mechanism solution, drilling-induced tensile fractures, overcoring, etc. (J. Reinecker et al., Borehole breakout analysis from four-arm caliper logs, 2004, http://www.world-stress-map.org)). *Sperner et al.* [2003] present a revised quality ranking criteria for stress orientations determined from breakouts calculated from four-arm caliper logs for the World Stress Map Project. The ranking scheme is based mainly on the number, accuracy, and length of measurements and is given in Table 1.

4. Results

[18] From the large number of wells drilled in the Neuquén Basin, 115 were identified as having all the necessary information needed for a borehole breakout analysis according to the procedure described in the previous section. For each well the four-arm caliper data were analyzed, identifying breakout segments and calculating the standard deviation of each breakout interval. It was also calculated the mean breakout orientation and the standard

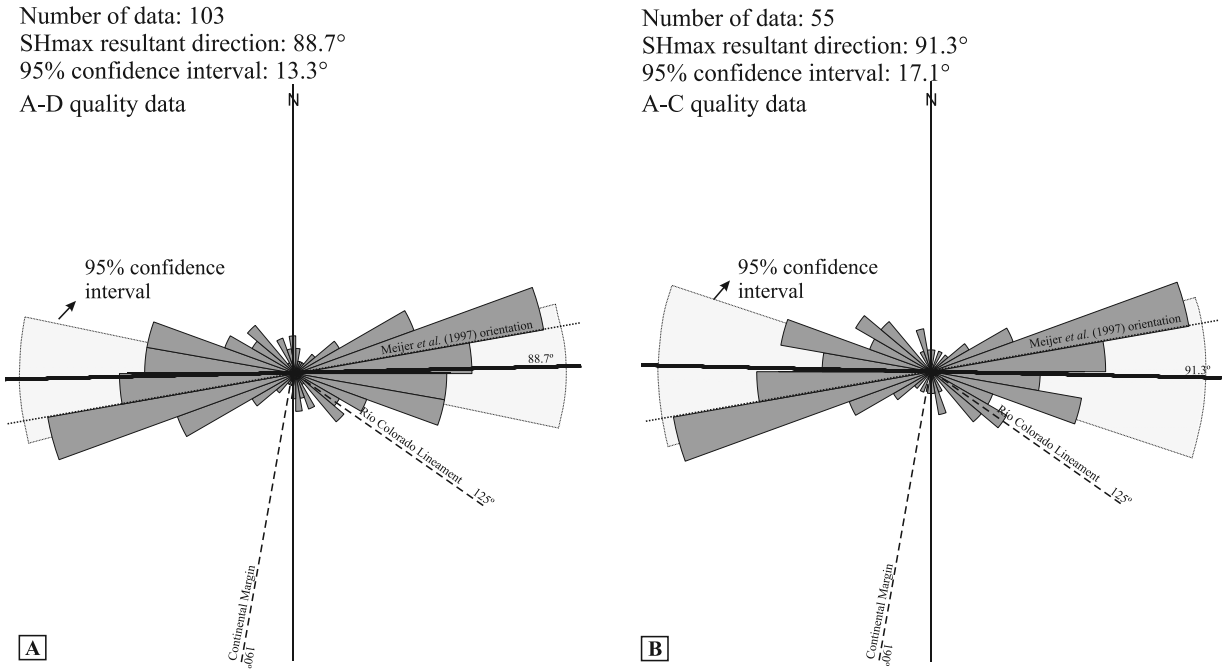

Figure 5. Rose diagram for the SH_{max} orientations. a) Rose diagram of all the data with qualities ranking from A to D. The distribution has a preference trend with a resultant direction of azimuth 88.7° and a 95% confidence interval of 13.3°. b) Rose diagram of all the data with qualities ranking from A to C. The distribution has a preference trend with a resultant direction of azimuth 91.3° and a 95% confidence interval of 17.1°. In dashed line there is plotted the SH_{max} direction achieved from *Meijer et al.* [1997].

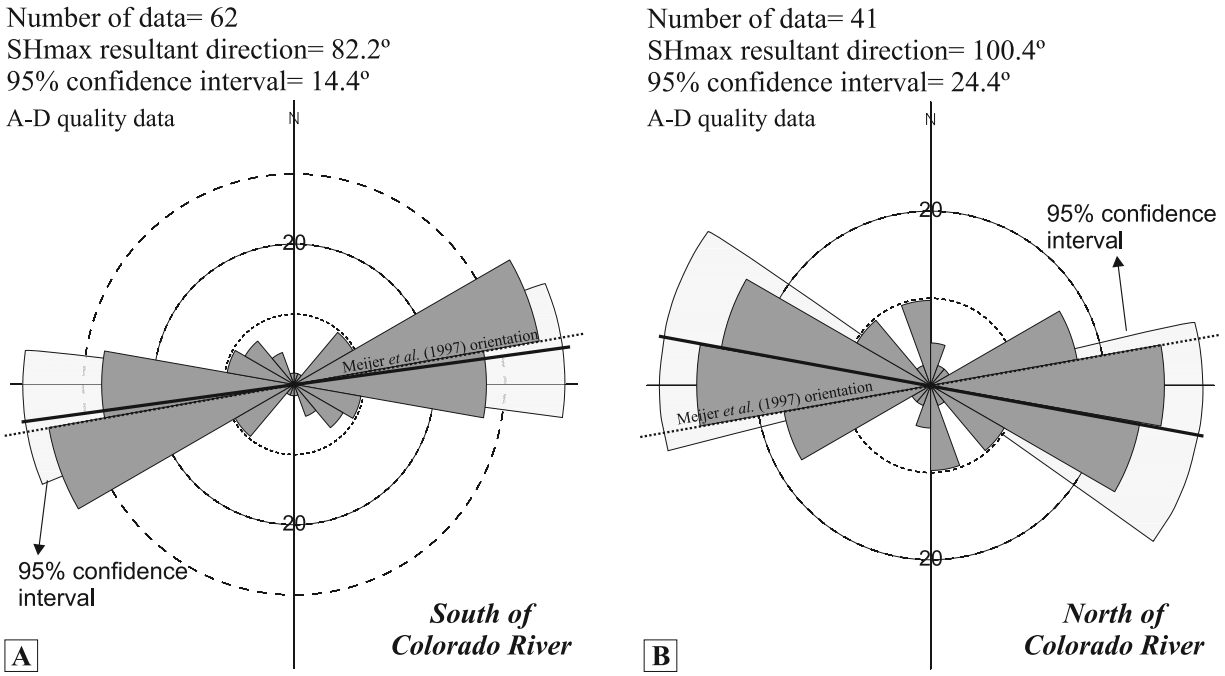

Figure 6. Rose diagram for the SH_{max} orientations using A–D quality data. a) South of the Colorado River, SH_{max} has a mean azimuth of 82.2°; b) North of the Colorado River, the SH_{max} has a mean azimuth of 100.4°. In dashed line there is plotted the SH_{max} direction achieved from *Meijer et al.* [1997].

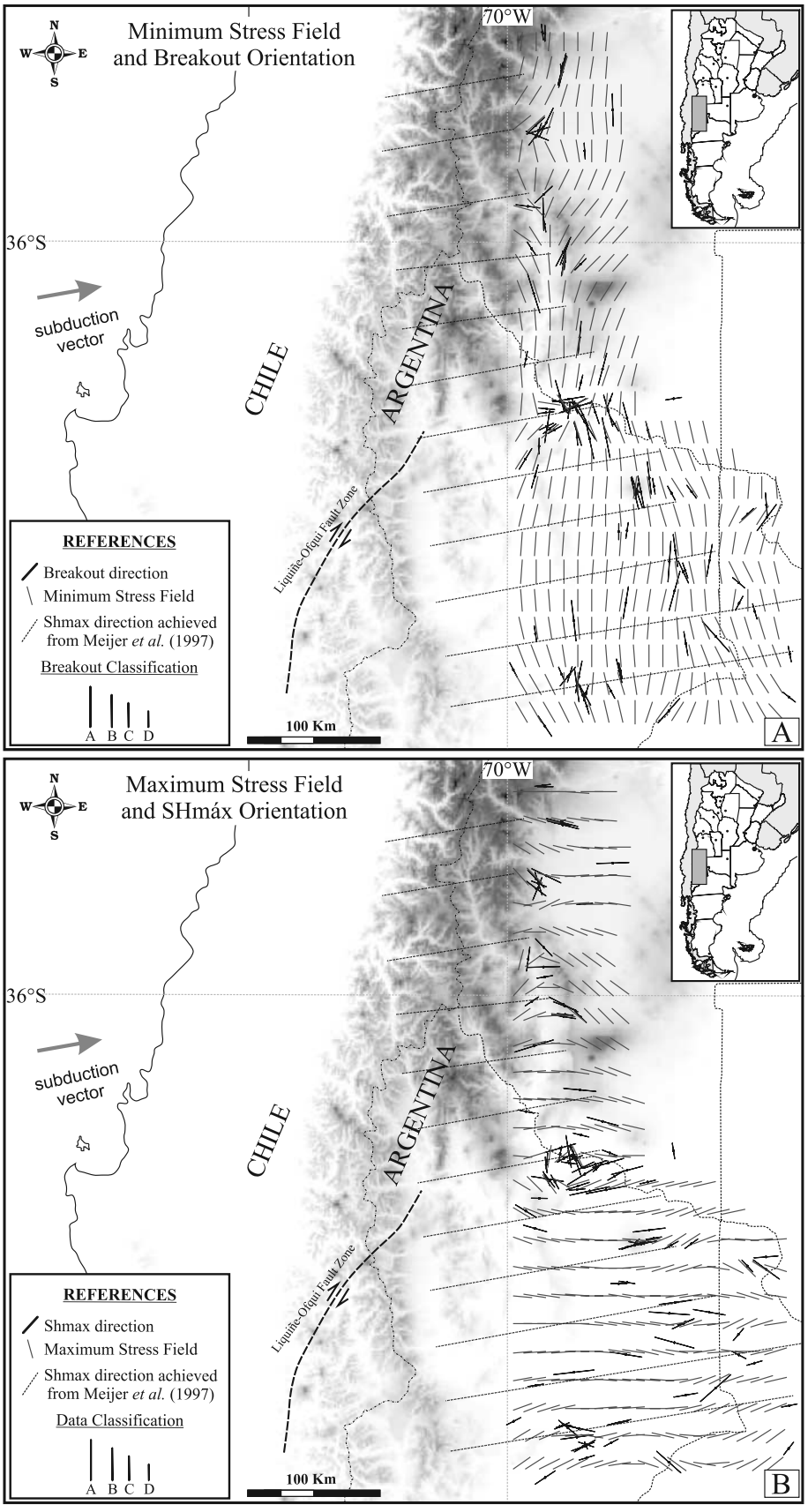
Minimum Stress Field
and Breakout Orientation
70°W
36°S
subduction
vector
CHILE
ARGENTINA
Liquiñe-Ofqui Fault Zone
REFERENCES
Breakout direction
Minimum Stress Field
Shmax direction achieved
from Meijer et al. (1997)
Breakout Classification
A B C D
100 Km
A
Maximum Stress Field
and SHmáx Orientation
70°W
36°S
subduction
vector
CHILE
ARGENTINA
Liquiñe-Ofqui Fault Zone
REFERENCES
Shmax direction
Maximum Stress Field
Shmax direction achieved
from Meijer et al. (1997)
Data Classification
A B C D
100 Km
B

Figure 7

deviation for the whole well. The data were classified using World Stress Map criterions (Table 1). Table 2 lists the 115 wells with their location, the mean breakout direction with its respective standard deviations (weighted by length and by number of breakout segments), the number of breakout intervals interpreted for each well, the accumulated length and the quality ranking.

[19] Breakout orientations are perpendicular to the maximum horizontal stress (SH_{max}) directions; therefore SH_{max} directions can be easily calculated. Figure 4 is a map with the SH_{max} orientation interpreted for the 115 wells analyzed in the Andean retroarc (Mendoza and Neuquén provinces of Argentina). The stress data are well distributed within the basin and give a coherent picture of SH_{max} orientation in the study area (Table 2 and Figure 4). Most of the SH_{max} orientations have a relative low to medium dispersion about the mean orientation; taking into account that 8 data were ranked as A, 25 as B, 22 as C, 48 as D, and 12 as E (see Tables 1 and 2). The data were recorded between depths of 17.3 and 4231 m.

[20] The SH_{max} orientations deduced from borehole breakout analysis have been plotted in two rose diagrams (Figure 5). In the first one (Figure 5a) only A–D quality data were used and in the second (Figure 5b) only A–C quality data. This means that in the second diagram the SH_{max} is accurate within ±25°. The distribution for the first diagram has a preferred trend with a resultant direction of azimuth 88.7° and a 95% confidence interval of 13.3°. The second one has a resultant direction of azimuth 91.3° and a 95% confidence interval of 17.1°. There are no significant differences between both mean directions and therefore all the data with quality ranking from A to D were used in the following analysis.

[21] In a general view, SH_{max} is oriented near E–W direction; however, it is not completely uniform within the whole area. The first observation is that to the north and south of the Colorado River there is a small, but significant difference. To the south the SH_{max} has a mean azimuth of 82.2° (Figure 6a) and to the north a mean azimuth of 100.4° (Figure 6b). The 95% confidence intervals of both populations are completely overlapped. The second observation is that data located southeast of the region tend to have a NE orientation, almost orthogonal to the Neuquén Basin boundary and the Colorado River bearing. Finally, there are some SE to N–S orientations placed to the west of the area near Colorado River and Sierra de Reyes (see Figures 2 and 4).

5. Interpretation and Discussion

[22] According to *Zoback* [1992] the first-order stress field pattern in an active continental margin is controlled by the plate boundary forces. For this sector of the Andean retroarc, the SH_{max} orientation should be controlled by the convergence vector between the Nazca and South American plates (azimuth 080°) [*Angermann et al.*, 1999; *Norabuena et al.*, 1999; *Kendrick et al.*, 2003], the direction of the ridge push (E–W) and the topographic forces (in general E–W, just perpendicular to the main topography axis). All of the forces are acting approximately with an E–W orientation in this segment of the South American Plate [*Coblentz and Richardson*, 1996; *Meijer et al.*, 1997]; therefore the expected SH_{max} orientation should be approximately parallel to them.

[23] In order to visualize the horizontal stress field in the studied region, a trajectory map (Figure 7) was made using the 103 A–D quality data. Figures 7a and 7b represent minimum (SH_{min}) and maximum (SH_{max}) horizontal stress fields, respectively. These maps show that the horizontal stress field along the study area is not completely uniform. However, its general trend is clearly consistent with the expected first-order present-day stress orientation (E–W). We use *Meijer et al.*'s [1997] model as reference frame for the expected stress field orientation, which incorporates topographic forces and a driving basal shear stress (Figure 7). The calculated SH_{max} (see Table 2 and Figure 5) are generally near the expected values. However, some deviations can be observed in the SH_{max} direction within the study area (Figure 4). Some possible explanations for these deviations are discussed below.

[24] It has already been pointed out that to the north and south of the Colorado River there is a small, but significant deviation of the SH_{max} orientation. To the south of Colorado River, the SH_{max} is almost parallel to the expected one (Figures 6a and 7) if plate boundary forces are considered as the principal ones (ENE direction). In this sector, the data are far from the high topographic front and a minor topographic influence is anticipated; however, the main topography axis of this segment has a NNW trend (Figure 7), reinforcing an ENE orientation for the SH_{max}.

[25] On the other hand, the stress data located to the north of the Colorado River deviate 11.7° counterclockwise from the mean 88.7° SH_{max} orientation (Figure 5a) prevailing in the region. The close relationship between stress trajectories and the topography (SH_{max} perpendicular to topography) observed for this sector suggests that either ancient structural indenters are controlling the horizontal stress field, or that topographic forces exert an important control on the stress field. The first hypothesis is consistent with the structure of this region where huge basement blocks are defining the NNE orogenic front of Malargüe fold and thrust belt and may be pushing the retroarc undeformed rocks. This idea is also coherent with *Brooks et al.* [2003] hypothesis of three plates, where an Andean microplate is modeled between Nazca and South American plates. A more complex shape for the Andean microplate than the one proposed by these authors should be used to explain

Figure 7. Trajectory maps of the minimum (a) and maximum (b) horizontal stress field constructed using the breakout and SH_{max} directions. To the north of Colorado River, the SH_{max} direction shows a tendency to be ESE. To the south the SH_{max} direction is more parallel to the ENE expected orientation. To the southeast of the region, a NE abnormal direction was found. In dashed lines there is the SH_{max} proposed by *Meijer et al.* [1997].

SH_{max} orientation of this region. However, Brooks et al. based their idea not only on measured velocity vectors but also on the abundant seismic activity concentrated in the front of the Andean microplate, just to the north of this region. For the study area, there is almost no seismic activity or neotectonic evidences in the orogenic front, indicating that this proposition may be not applicable to this part of the Andean retroarc.

[26] The second situation was proposed and justified by other authors [*Coblentz and Richardson*, 1996; *Meijer et al.*, 1997] and could also be supported by these SH_{max} orientation. Figure 7 reveals that stress data located to the north of the Colorado River are closer to the high topographic front than those placed to the south of Colorado River and that the topographic axis of this Andean segment has a NNE bearing consistent with inducing an ESE SH_{max} direction.

[27] To the southeast of the region, a NE direction was found (Figure 7), this orientation can be interpreted as the response to a regional basement structural control. *Cristallini et al.* [2006] have shown that the principal Triassic-Jurassic half graben faults of the northeastern Neuquén Basin have a NW trend, parallel to the minimum horizontal stress orientation found for this sector. The Neuquén Basin boundary also has the same direction and is parallel to the Río Colorado lineament. In the same way, the Triassic-Jurassic synrift transference zones in this region have a NE orientation, parallel to the maximum horizontal stress.

[28] Finally, there are some SH_{max} orientation, especially to the west, close to Sierra de Reyes and Río Colorado, which are not following the regional trend (Figure 4). These are probably controlled by local perturbations due to local structures, because most of them are inside the fold and thrust belt zone where the structure is more complex than in the foreland. In addition, *Folguera et al.* [2005] have shown that some NNW trending tensional basins are overprinted on the fold and thrust belt region during Quaternary. These structures, together with SH_{max} rotations near complex structures, can explain these data.

6. Conclusions

[29] The principal horizontal stress orientations acting in the Andean retroarc between 34° and 39°S have been calculated using breakout information interpreted from dipmeter logs of 115 wells drilled in the Neuquén Basin along Neuquén and Mendoza provinces of Argentina. A resultant mean SH_{max} orientation of 88.7° and a 95% confidence interval of 13.3° were calculated for the whole area. The breakout information of each well was quality ranked using the World Stress Map Project criterions and a map of the maximum and minimum horizontal stress fields was made based on 103 wells obtained after rejecting low-quality data (see Figure 7).

[30] The obtained stress direction (Figure 7) is generally aligned with the subduction vector of the Nazca plate and perpendicular to the topography. This is consistent with model 2 of *Coblentz and Richardson* [1996] which considered a fixed collisional boundary and topographic forces associated with elevated continental crust and with *Meijer et al.* [1997] model which also assesses the topographic forces and assumes a driving basal shear stress of 0.5 MPa (Figure 7). From the comparison of the data obtained in this research with the models presented by *Coblentz and Richardson* [1996] and *Meijer et al.* [1997], it can be seen that the topographic, the plate boundary and the basal drag forces could be mainly controlling the stress field. Likewise, it is difficult to discern which of these forces is the mainly responsible for the stress alignment since they are all almost acting in the same direction.

[31] Zooming into local scales some deviations from the general E–W pattern are observed. To the north of Colorado River, the SH_{max} shows an ESE tendency (Figures 6b and 7) and to the southeast of the region a NE direction was found (Figure 7). These local perturbations due to forces induced by local non meridian topographic axis or to basement controls lead to small rotations with respect to the general trend.

[32] **Acknowledgments.** We want to express our gratitude to Repsol-YPF for providing the data needed for this research. This study has been done with funding from Agencia Nacional de Promoción Científica y Tecnológica, CONICET (PEI 6465/04 and PEI 5758/05) and Universidad de Buenos Aires (01/X160). In addition, we particularly acknowledge Mark Tingay, namely, for the reviews and important contributions to this research, and Victor Ramos for previous reviews of this paper. We also want to acknowledge the reviewers Oliver Heidbach and Benjamin Brooks for providing a highly constructive evaluation.

References

Angermann, D., J. Klotz, and C. Reigber (1999), Space-geodetic estimation of the Nazca-South America Euler vector, *Earth Planet. Sci. Lett.*, *171*, 329–334.

Babcock, E. A. (1978), Measurement of surface fractures from dipmeter logs, *Am. Assoc. Pet. Geol. Bull.*, *62*(7), 1111–1126.

Barrio, C. A. (1990), Late Cretaceous–early Tertiary sedimentation in a semi-arid foreland basin (Neuquén Basin, western Argentina), *Sediment. Geol.*, *66*, 255–275.

Bell, J. S., and E. A. Babcock (1986), The stress regime of the Western Canadian Basin and the implications for hydrocarbon production, *Bull. Can. Pet. Geol.*, *34*(3), 364–378.

Bell, J. S., and D. I. Gough (1979), Northeast–southwest compressive stress in Alberta: Evidence from oil wells, *Earth Planet. Sci. Lett.*, *45*, 475–482.

Bell, J. S., and D. I. Gough (1982), The use of borehole breakouts in the study of crustal stress, *U.S. Geol. Surv. Open File Rep.*, *82-1075*, 539–557.

Brooks, B. A., M. Bevis, R. Smalley Jr., E. Kendrick, R. Manceda, E. Lauría, R. Maturana, and M. Araujo (2003), Crustal motion in the Southern Andes (26°–36°S): Do the Andes behave like a microplate?, *Geochem. Geophys. Geosyst.*, *4*(10), 1085, doi:10.1029/2003GC000505.

Cobbold, P. R., and E. A. Rossello (2003), Aptian to recent compressional deformation, foothills of the Neuquén Basin, Argentina, *Mar. Pet. Geol.*, *20*, 429–443.

Cobbold, P. R., M. Diraison, and E. A. Rossello (1999), Bitumen veins and Eocene transpression, Neuquén Basin, Argentina, *Tectonophysics*, *14*, 423–442.

Coblentz, D. D., and R. M. Richardson (1996), Analysis of the South American intraplate stress field, *J. Geophys. Res.*, *101*, 8643–8657.

Cortés, J. M. (2000), Fallas cuaternarias oblicuas al frente montañoso en la Cordillera Frontal de Mendoza (34°34′30′S), *Asoc. Geol. Argent. Rev., Ser. D Publ. Especial*, *4*, 57–62.

Cox, J. W. (1970), The high resolution dipmeter reveals dip–related borehole and formation characteristics, *Trans. SPWLA Annu. Logging Symp.*, *11*, 3–6.

Cristallini, E. O., G. Bottesi, A. Gavarrino, L. Rodríguez, R. Tomezzoli, and R. Comeron (2006), Synrift geometry of the Neuquén Basin in northeastern Neuquén Province, Argentina, in *Evolution of an Andean Margin: A Tectonic and Magmatic View From the Andes to the Neuquén Basin (36–39°S lat)*, edited by S. M. Kay and V. A. Ramos, *Spec. Pap. Geol. Soc. Am.*, *407*, 147–161.

Dalmayarc, B., and P. Molnar (1981), Parallel thrust and normal faulting in Peru and constraints on the state of stress, *Earth Planet. Sci. Lett.*, *55*, 473–481.

Folguera, A., V. Ramos, and D. Melnick (2002), Partición de la deformación en la zona del arco volcánico de los Andes neuquinos en los últimos 30 millones de años (36°–39°S), *Rev. Geol. Chile*, *29*(2), 151–165.

Folguera, A., V. Ramos, T. R. Zapata, M. Spagnuolo, and F. Miranda (2005), Pliocene to Quaternary retro-arc extension in the Andes at 35°–37°30′S, paper presented at 6th International Symposium on Andean Geodynamics, Inst. de Rec. Puor le Dév., Barcelona.

Fuchs, K., and B. Müller (2001), World stress map of the Earth: A key to tectonic processes and technological applications, *Naturwissenschaften*, *88*, 357–371.

Gough, D. I., and J. S. Bell (1979), Stress orientations from borehole wall fractures with examples from Colorado, east Texas and northern Canada, *Can. J. Earth Sci.*, *19*, 1358–1370.

Gough, D. I., and J. S. Bell (1981), Stress orientations from oil well fractures in Alberta and Texas, *Can. J. Earth Sci.*, *18*, 638–645.

Kay, S. M. (2005), Tertiary to Recent evolution of Andean arc and backarc magmas between 36°S and 38°S and evidence for Miocene shallowing of the Nazca plate under the Neuquén Basin, paper presented at 6th International Symposium on Andean Geodynamics, Inst. de Rec. Puor le Dév., Univ. de Barcelona, Inst. Geol. y Minero de Esp., Barcelona.

Kendrick, E., M. Becis, R. Smalley Jr., B. Brooks, R. B. Vargas, E. Lauría, and L. P. Souto Fortes (2003), The Nazca-South America Euler vector and its rate of change, *J. South Am. Earth Sci.*, *16*, 125–131.

Kozlowski, E. E. (1991), Structural geology of the NW Neuquén Basin, Argentina, paper presented at IV Simposio Bolivariano, Explor. Pet. en las Cuencas Subandinas, Bogotá, Colombia.

Kozlowski, E. E., C. Cruz, P. Condal, and R. Manceda (1990), Modelo estructural para el zócalo de la Cuenca Neuquina, Mendoza, Argentina, paper presented at XI Congreso Geológico Argentino, Asoc. Geol. Argent., San Juan.

Kozlowski, E. E., R. Manceda, and V. Ramos (1993), Estructura, in *Geología y Recursos Naturales de Mendoza*, edited by V. A. Ramos, *Rep. I*(18), pp. 235–256, Asoc. Geol. Argent., Buenos Aires, Argentina.

Lavenu, A., and J. Cembrano (1999a), Compressional and transpressional stress pattern for Pliocene and Quaternary brittle deformation in fore arc and intra arc zones (Andes of central and southern Chile), *J. Struct. Geol.*, *21*(12), 1669–1691.

Lavenu, A., and J. Cembrano (1999b), Estados de esfuerzo compresivo plioceno y compresivo-transpresivo pleistoceno, Andes del sur, Chile (38°–42°30′S), *Rev. Geol. Chile*, *26*(1), 67–87.

Legarreta, L., and M. A. Uliana (1996), The Jurassic succession in west-central Argentina: Stratal patterns, sequences and paleogeographic evolution, *Palaegeogr. Palaeoclimatol. Palaeoecol.*, *120*, 303–330.

Legarreta, L., D. A. Kokogian, and C. A. Gulisano (1989), Depositional sequences of the Malargüe Group (Upper Cretaceous–Lower Tertiary), Neuquén Basin, Argentina, *Cretaceous Res.*, *10*, 337–356.

Manceda, R., and D. Figueroa (1995), Inversion of Mesozoic Neuquén rift in the Malargüe fold and thrust belt, Mendoza, Argentina, in *Petroleum Basins of South America*, edited by A. J. Tankard, R. Suárez, and H. J. Welsnik, *AAPG Mem.*, *62*, 369–382.

Meijer, P. T., R. Govers, and M. J. R. Wortel (1997), Forces controlling the present-day state of stress in the Andes, *Earth Planet. Sci. Lett.*, *148*, 157–170.

Mendiberri, H., and O. Carbone (2002), Cuenca Neuquina: Marco geológico y reseña histórica de la actividad petrolera, in *Rocas Reservorio de las Cuencas Productivas de la Argentina*, edited by M. Schiuma, G. Hinterwiummer, and G. Vergani, pp. 201–211, Inst. Arg. del Petrol. y del Gas, Buenos Aires, Argentina.

Mosquera, A. (2002), Inversión tectónica Jurásico Inferior en el sector central de la dorsal de Huincul, área Los Bastos, paper presented at V Congreso de Exploración y Desarrollo de Hidrocarburos, Asoc. Argent. de Geól. y Geofís. Petrol., Mar del Plata, Argentina.

Mosquera, A., and V. Ramos (2005), Intraplate deformation in the Neuquén embayment, paper presented at XVI Congreso Geológico Argentino, Asoc. Geol. Argent., La Plata, Argentina.

Muñoz, J., and C. Stern (1988), The Quaternary volcanic belt of the southern continental margin of South America: Transverse structural and petrochemical variations across the segment between 38°S and 39°S, *J. South Am. Earth Sci.*, *1*(2), 147–161.

Muñoz, J., R. Troncoso, P. Duhart, P. Crígnola, L. Farmer, and C. Stern (2000), The relationship of the mid-Tertiary coastal magmatic belt in south-central Chile to the late Oligocene increase in plate convergence rate, *Rev. Geol. Chile*, *27*(2), 177–203.

Norabuena, E., T. Dixon, S. Stein, and C. G. A. Harrison (1999), Decelerating Nazca-South America and Nazca-Pacific motions, *Geophys. Res. Lett.*, *26*, 3405–3408.

Pángaro, F., R. Veiga, and G. Vergani (2002), Evolución tecto–sedimentaria del área de Cerro Bandera, Cuenca Neuquina, Argentina, paper presented at V Congreso de Exploración y Desarrollo de Hidrocarburos, Asoc. Argent. de Geól. y Geofís. Petrol., Mar del Plata, Argentina.

Ploszkiewicz, J. V. (1987), Las zonas triangulares de la faja fallada y plegada de la Cuenca Neuquina Argentina, paper presented at X Congreso Geológico Argentino, Asoc. Geol. Argent., San Miguel de Tucumán, Argentina.

Plumb, R. A., and J. W. Cox (1987), Stress directions in eastern North America determined to 4.5 km from borehole elongation measurements, *J. Geophys. Res.*, *92*, 4805–4816.

Plumb, R. A., and S. H. Hickman (1985), Stress induced borehole elongation: A comparison between four arm dipmeter and the borehole televiewer in the Auburn Geothermal Well, *J. Geophys. Res.*, *90*, 5513–5521.

Ramos, V. A. (1989), The birth of southern South America, *Am. Sci.*, *77*, 444–450.

Ramos, V. A. (1998), Estructura del sector occidental de la faja plegada y corrida del Agrio, Cuenca Neuquina, Argentina, paper presented at X Congreso Latinoamericano de Geología and VI Congreso Nacional de Geología Económica, Asoc. de Serv. Geol. y Mineros de Iberoam., Buenos Aires, Argentina.

Ramos, V. A., and A. Folguera (2005a), Tectonic evolution of the Andes of Neuquén: Constraints derived, from the magmatic arc and foreland deformation, in *The Neuquén Basin, Argentina: A Case Study in Sequence Stratigraphy and Basin Dynamics*, edited by G. D. Veiga et al., *Geol. Soc. Spec. Publ.*, *252*, 15–35.

Ramos, V. A., and A. Folguera (2005b), El origen de Payenia (Mendoza sur y norte de Neuquén): Evolución estructural y tectonomagmática de los Andes a estas latitudes, paper presented at XVI Congreso Geológico Argentino, Asoc. Geol. Argent., La Plata, Argentina.

Ramos, V. A., M. Cegarra, and E. O. Cristallini (1996), Cenozoic tectonics of the high Andes of west-central Argentina (30°–36°S latitude), *Tectonophysics*, *259*, 185–200.

Richardson, R. M., and D. D. Coblentz (1994), Stress modelling in the Andes: Constraints on South American intraplate stress magnitudes, *J. Geophys. Res.*, *99*, 22,015–22,025.

Sperner, B., B. Müller, O. Heidbach, D. Delvaux, J. Reinecker, and K. Fuchs (2003), Tectonic stress in the Earth's crust: Advances in the World Stress Map Project, in *New Insights Into Structural Interpretation and Modeling*, edited by D. Nieuwland, *Geol. Soc. Spec. Publ.*, *212*, 101–116.

Stern, C. (1989), Pliocene to present migration of the volcanic front, Andean Southern Volcanic Front, *Rev. Geol. Chile*, *16*(2), 145–162.

Tingay, M., B. Müller, J. Reinecker, O. Haidbach, F. Wenzel, and P. Fleckenstein (2005), The World Stress Map Project "Present-day stress in sedimentary basins" initiative: Building a valuable public resource to understand tectonic stress in the oil patch, *Leading Edge*, *24*(12), 1276–1282.

Turic, M., F. Aramayo Flores, R. Gómez Omil, R. Pombo, G. Peroni, J. Sciutto, D. Robles, and A. Cáceres (1987), Geología de las cuencas petroleras de la Argentina, in *Evaluación de las Formaciones en la Argentina*, vol. I(1), edited by S. A. Felder, p. 144, Schlumberger, Buenos Aires.

Uliana, M. A., M. E. Arteaga, L. Legarreta, J. J. Cerdán, and G. Peroni (1995), Inversion structures and hydrocarbon ocurrentes in Argentina, in *Basin Inversion*, edited by J. G. Buchman and P. G. Buchman, *Geol. Soc. Spec. Publ.*, *88*, 211–233.

Vergani, G. D., A. J. Tankard, H. J. Belotti, and H. J. Welsink (1995), Tectonic evolution and paleogeography of the Neuquén Basin, Argentina, in *Petroleum Basins of South America*, edited by A. J. Tankard, R. Suárez, and H. J. Welsink, *AAPG Mem.*, *62*, 383–402.

Viñes, R. (1990), Productive duplex imbrication at the Neuquén Basin thrust belt front, Argentina, in *Petroleum and Tectonics in Mobile Belts*, edited by J. Letouzey, pp. 69–80, Technip, Paris.

Yagupsky, D. L., E. O. Cristallini, G. Zamora Valcarce, and R. Varadé (2007), Sistema compresivo sobreimpuesto a un rift oblicuo: Aplicaciones en la faja plegada y corrida de Malargüe, sur de Mendoza, *Rev. Asoc. Geol. Argent.*, in press.

Zajac, B. J., and J. M. Stock (1997), Using borehole breakouts to constrain the complete stress tensor: Results from the Sijan Deep Drilling Project and offshore Santa Maria Basin, California, *J. Geophys. Res.*, *102*, 10,083–10,100.

Zamora Valcarce, G., T. Zapata, and D. del Pino (2005), Edad de la deformación y magmatismo en la faja plegada del Agrio, paper presented at XVI Congreso Geológico Argentino, Asoc. Geol. Argent., La Plata, Argentina.

Zapata, T., I. Brissón, and F. Dzelalija (1999), La Estructura de la faja plegada y corrida andina en relación con el basamento de la Cuenca Neuquina, *Bol. Inf. Pet.*, *60*, 112–121.

Zerwer, A., and N. A. Yassir (1994), Borehole breakout interpretation in the Gulf Coast, offshore Louisiana, in *Rock Mechanics*, edited by P. P. Nelson and S. E. Laubach, pp. 225–232, A. A. Balkema, Rotterdam, Netherlands.

Zoback, M. D., and M. L. Zoback (1991), Tectonic stress field of North America and relative plate motions, in *Neotectonics of North America Decade Map, Volume I*, edited by D. B. Slemmons et al., pp. 339–366, Geol. Soc. of Am., Boulder, Colo.

Zoback, M. D., D. Moss, L. G. Mastin, and R. N. Anderson (1985), Well bore breakouts and in situ stress, *J. Geophys. Res.*, *90*, 5523–5530.

Zoback, M. L. (1992), The first and second order patterns of stress in the lithosphere: The World Stress Map Project, *J. Geophys. Res.*, *97*, 11,703–11,728.

Zoback, M. L., and M. D. Zoback (1989), Tectonic stress field of the conterminous United States, in *Geophysical Framework of the Continental United States*, edited by L. C. Pakiser and W. D. Mooney, *Mem. Geol. Soc. Am.*, *172*, 523–539.

Zoback, M. L., et al. (1989), Global patterns of tectonic stress, *Nature*, *341*, 291–298.

G. Bottesi, Repsol YPF, Esmeralda 255, Piso 10, Oficina 101E, Buenos Aires C1035ABE, Argentina.

E. Cristallini and C. Guzmán, Laboratorio de Modelado Geológico, Departamento de Ciencias Geológicas, Universidad de Buenos Aires, Pabellón II, Buenos Aires C1428EHA, Argentina. (ceciliagguzman@hotmail.com)